JOURNAL OF THERMOPHYSICS AND HEAT TRANSFER
Vol. 20, No. 1, January–March 2006

Elemental Demixing in Inductively Coupled Air Plasma Torches at High Pressures

P. Rini*
von Kármán Institute for Fluid Dynamics (VKI), 1640 Rhode-St.-Genèse, Belgium
and
D. Vanden Abeele† and G. Degrez‡
Université Libre de Bruxelles (ULB), 1050 Bruxelles, Belgium

We present and analyze detailed numerical simulations of high-pressure inductively coupled air plasma flows using two different mathematical formulations: an extended chemical non-equilibrium formalism including finite-rate chemistry and a form of the equations valid in the limit of local thermodynamic equilibrium and accounting for the demixing of chemical elements. Simulations at various operating pressures indicate that significant demixing of oxygen and nitrogen occurs, regardless of the degree of nonequilibrium in the plasma. Ideally, this effect should therefore be taken into account when the results of tests of thermal protection materials for (re-)entry spacecraft in inductively coupled plasma wind tunnels are processed. As the operating pressure is increased, chemistry becomes increasingly fast and the nonequilibrium results correctly approach the results obtained assuming local thermodynamic equilibrium, supporting the validity of the proposed local equilibrium formulation.

Nomenclature

A_s = symbolic notation for species s
h = mixture-specific enthalpy
h_i = specific enthalpy of species i
$\boldsymbol{J}_i$ = mass diffusion flux of species i
$\mathcal{J}_c$ = mass diffusion flux of element c
K_c = equilibrium constant
k_f = forward reaction rate
k_b = backward reaction rate
M_i = molar mass of species i
N_{el} = number of elements
N_{ic} = number of independent components
N_r = number of dependent components
N_{sp} = number of species
p = mixture pressure
$\mathcal{Q}_s$ = charge of species s
T = mixture temperature
u = z-component of the velocity
$\boldsymbol{u}$ = mixture velocity
v = r-component of the velocity
w = θ-component of the velocity
Y_c = mass fraction of element c
y_s = mass fraction of species s
X_c = volumetric fraction of element c
x_s = mole fraction of species s
μ = mixture dynamic viscosity
ν'_{sr} = stoichiometric coefficient of species s as a reactant in reaction r
ν''_{sr} = stoichiometric coefficient of species s as a product in reaction r
ρ = mixture density
ρ_s = partial density of species s
σ = electrical conductivity
ϕ_s^c = number of elements of type c in the species s
$\dot{\omega}_s$ = mass production/destruction of species s due to chemical reactions

Presented as Paper 2004-2472 at the AIAA 37th Thermophysics Conference, Portland, OR, 28 June–1 July 2004; received 1 February 2005; revision received 20 April 2005; accepted for publication 21 April 2005.

*Ph.D. Candidate, Department of Aeronautics and Aerospace, 72, Ch. de Waterloo; also Assistant, Université Libre de Bruxelles, Service de Mécanique des Fluides, 50, Avenue F. D. Roosevelt, 1050 Bruxelles, Belgium; rini@vki.ac.be. Member AIAA.

†Researcher, Service de Mécanique des Fluides, 50, Avenue F. D. Roosevelt; david.vanden.abeele@ulb.ac.be. Member AIAA.

‡Professor, Service de Mécanique des Fluides, 50, Avenue F. D. Roosevelt; also Adjunct Professor, von Kármán Institute, Department of Aeronautics and Aerospace, 72, Ch. de Waterloo, 1640, Rhode-St.-Genèse, Belgium; gdegrez@ulb.ac.be. Associate Fellow AIAA.

Introduction

MODELING collision-dominated chemically reacting flows requires the solution of an extended Navier–Stokes formalism, consisting of the following equations:[1] 1) global continuity, momentum, and total energy; 2) a separate continuity equation for each species, including finite-rate chemistry; 3) if thermal nonequilibrium occurs, a continuity equation for each mode. This system of equations is hard to implement and solve numerically. In addition, many physical parameters essential for the modeling of kinetic and chemical processes in the gas mixture are usually missing or uncertain. For these reasons, when chemistry and energy exchanges are fast, it is usually preferable to solve the more elegant and reliable local thermodynamic equilibrium (LTE) form of the aforementioned set of equations. A major breakthrough in the field of LTE flow modeling was made by Butler and Brokaw[2] and Brokaw,[3] who showed that, assuming vanishing diffusive fluxes of chemical elements, the diffusive transport of reaction enthalpy in the energy equation can be incorporated in a trivial manner by introducing a coefficient of "thermal reactive conductivity":

$$\sum_{s=1}^{N_{\text{sp}}} \boldsymbol{J}_s h_s = -\lambda_r^{\text{BB}} \nabla T \tag{1}$$

Often, one makes use of this result to reduce the full set of nonequilibrium equations to a system formally equivalent to the "conventional" Navier–Stokes equations (continuity, momentum, and energy), complemented by a modified equation of state $\rho(p, T)$ computed from statistical mechanics assuming a fixed elemental composition in the flow. For instance, Vasil'evskii et al.,[4] Vanden Abeele and Degrez,[5] and Magin and Degrez[6] successfully used this straightforward LTE formalism to simulate high-pressure air inductively coupled plasma flows.

Although this approach is appealing because of its simplicity, it is important to understand that it is approximate at best, because in general the elemental composition varies significantly in chemically reacting flows. Consider, as a striking example, LTE diffusion flames in which fuel and air are injected through different inlets and gradually mix. Even in favorable situations, where initial species compositions vary in such a manner that the elemental composition is uniform, the rigorous kinetic theory in general predicts nonzero element diffusion fluxes, which spontaneously lead to a certain degree of "demixing" of elements. At present, we know of no chemically reacting mixture containing more than a single element that can simultaneously satisfy the constraints of uniform elemental composition and vanishing elemental fluxes when chemical reactions take place.

Over the past forty years, several LTE formulations accounting for demixing effects have been proposed and some of them have been applied to describe flow conditions of interest in both aerospace sciences and applied physics:

1) Suslov et al.[7] presented a general theoretical description of mixtures of chemically reacting gases under chemical equilibrium for which (de-)mixing is taken into account by solving a set of elemental continuity equations. This formulation has been further improved in two more recent papers due to G. A. Tirsky[8,9] and represents the most complete and accurate description of LTE flows presently available.

2) Murphy[10–13] has investigated effects of elemental demixing in thermal arc-plasmas and points out that demixing occurs regardless of the degree of nonequilibrium in the plasma. Thus, even in the LTE case, an additional continuity equation needs to be included for each element in the gas mixture. He presents an approximate LTE model that makes it possible to compute demixing in binary mixtures of homonuclear gases, which do not mutually react. Although rigorous, his model cannot be applied to the more general case where species composed of various nuclei appear. For instance, an air plasma, which consists of nitrogen and oxygen nuclei, will contain mixed species such as NO that cannot be described by this theory. In addition, different species do react in general.

3) Van der Heijden[14] has proposed an alternative LTE model in his study of demixing in a Hg/Na/I metal halide lamp. His formulation is based upon a Fick-type diffusion model, which can only be applied when a minority species diffuses with respect to a background species, which is present in overwhelming quantities (mercury, in his case).

4) Rini and Degrez[15] recently performed calculations of air and carbon dioxide stagnation line flows under LTE using a formulation similar to that of Suslov et al.[7] For each chemical element an additional continuity equation is solved at each iteration in the numerical solution procedure. The species diffusion fluxes are calculated explicitly by solving the system of Stefan–Maxwell[16,17] equations. From the species diffusion fluxes, one computes the elemental diffusion fluxes that appear in the elemental continuity equations, as well as the diffusive enthalpy transport in the energy equation. The pressure, velocity, temperature, and elemental concentration fields are updated for given values of the aforementioned diffusive terms.

5) Finally, Rini et al.[18] derived an explicit closed form of the equations for chemically reacting flows of neutral species under LTE, in which the diffusion fluxes of elements and species enthalpies are expressed as explicit linear functions of gradients of elemental mass fractions, pressure and temperature.

In this contribution, the approach of Rini and Degrez[15] is extended to mixtures of partially ionized gases to investigate demixing of oxygen and nitrogen elements in high-pressure air inductively coupled plasmas (ICPs) close to LTE.

An ICP torch is a device that makes it possible to heat gases to temperatures of ~10,000 K in a clean electrodeless manner. The gas is injected into a quartz tube surrounded by a copper inductor. A radio frequency electrical current runs through the inductor and induces a secondary current through the gas inside the quartz tube, which heats up by means of ohmic dissipation. High-pressure ICPs are rather close to equilibrium, in contrast with low-pressure inductive discharges, in which nonequilibrium (NEQ) processes play a dominant role.[19]

The motivation of the present contribution is twofold:

1) It is common practice in aerospace sciences to compute LTE flows, assuming a fixed elemental composition. Care should be taken in comparing these results with nonequilibrium calculations, for which demixing of elements does occur: are the observed differences due to nonequilibrium effects, or simply a consequence of the fact that demixing is not taken into account in the LTE model? The results to be presented clearly show that as pressure is increased and equilibrium conditions are approached, differences between the fixed elemental fraction LTE model and the nonequilibrium model persist; however, when variations of elemental composition are correctly allowed for in the LTE model, excellent agreement is found.

2) In the aerospace industry, and in particular at the von Kármán Institute for Fluid Dynamics, high-pressure air ICPs are used to test thermal protection system (TPS) materials for atmospheric (re-)entry spacecraft. In these tests, the surface catalyticity properties of the material undergoing testing are evaluated by means of a hybrid experimental–numerical methodology based on the local heat transfer simulation concept,[20] which relies heavily upon the numerical simulation of the air ICP used. Although we do not question the adequacy of the LTE assumption used for these simulations by the Russian specialists who originally developed this methodology, we wish to point out that, to obtain accurate results under general operating conditions, the demixing of chemical elements should be included in the LTE model.

Although we will focus on the particular case of high-pressure air ICP torches in this paper, we wish to point out that the presented LTE formulation is applicable to any chemically reacting flow near LTE, in particular the hydrocarbon–air mixtures used for combustion.

Governing Equations

We represent the air plasma by a mixture of 11 chemical components, suited for Earth entry applications[21]: 1) Neutral species: O_2, N_2, O, N, NO; 2) Charged species: NO^+, O^+, N^+, O_2^+, N_2^+, e^-.

As mentioned and justified in Ref. 5, in high-pressure air ICPs we find that[22]

1) The plasma is strongly collision-dominated and may be described with a Navier–Stokes type fluid model.

2) magnetic fields are relatively weak, so that the gyroradii of charged particles exceed their mean free paths by one or more orders of magnitude. The plasma transport properties are then isotropic and Hall currents may be neglected.

3) The Debye length is small compared to the torch-dimensions. The plasma may therefore be considered quasi-neutral.

4) The plasma frequency by far exceeds the operating frequency of the torch. A magneto-hydrodynamic (MHD) description of the plasma is thus justified.

Although we incorporate general chemical nonequilibrium effects, we make the working assumption that the plasma is at thermal equilibrium. Although this is rarely the case at low operating pressures,[5] the inclusion of thermal nonequilibrium would not add anything to the discussion in this paper, which exclusively addresses issues of chemical nonequilibrium. We wish to stress that the same conclusions would be obtained if, in addition, thermal nonequilibrium were included in our nonequilibrium simulations.

We will now present the governing electromagnetic and flow equations for high-pressure ICPs under thermal equilibrium. For a more general description including thermal nonequilibrium, we refer the reader to our previously published work.[5]

Electromagnetics

The VKI Plasmatron torch geometry used in the present simulations is shown in Fig. 1. The torch is modeled by a fully axisymmetric configuration by approximating the (solenoidal) inductor by a series of n_c parallel, current-carrying rings. For simplicity, we assume the rings to be infinitely thin current loops, located at the innermost part of the true coil rings, where most of the electric current is known to run.[5]

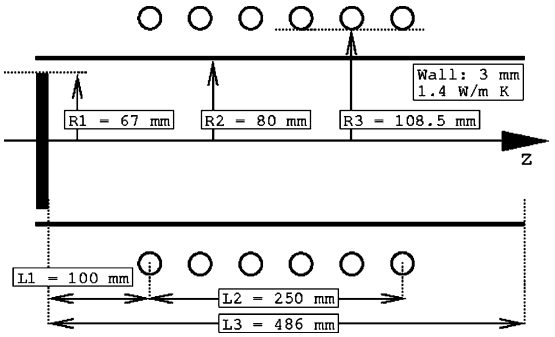

Fig. 1 VKI plasmatron torch geometry.

External Current Density

For the radio frequencies typically used in ICPs, it is reasonable to assume that a single current with amplitude I_c and frequency f oscillates at phase-angle zero through each coil ring.[23] The external current density amplitude J_V then reads

$$J_V = -I_c \sum_{i=1}^{n_c} \delta(\boldsymbol{r} - \boldsymbol{r}_i) \tag{2}$$

where the Dirac distribution $\delta(\boldsymbol{r} - \boldsymbol{r}_i)$ takes care of the singular current density in the ith loop.

Assumption of Vanishing Poloidal Electrical Current

Inside the plasma, powerful induced currents oscillate in the toroidal (θ) direction. In the poloidal (r–z) plane, in contrast, we make the reasonable assumption that electrical currents vanish.[4,5]

MHD Induction Equation

The induced electric field $\boldsymbol{E}$ is purely toroidal and consists of a single Fourier mode at the torch operating frequency:

$$\boldsymbol{E} = E \exp(i\, 2\pi f t)\, \boldsymbol{e}_\theta \tag{3}$$

Because the magnetic Reynolds number is small, the electric field satisfies the following Helmholtz-type MHD induction equation, both inside the torch and on a far-field domain covering the space around the torch[24]:

$$\frac{\partial^2 E}{\partial z^2} + \frac{1}{r}\frac{\partial}{\partial r}\left(r\frac{\partial E}{\partial r}\right) - \frac{1}{r^2}E - i\mu_0 2\pi f \sigma E = i\mu_0 2\pi f J_V \tag{4}$$

where μ_0 represents the magnetic permeability of free space. To take into account phase differences inside the torch, E stands for a complex variable.

The electric field amplitude should be zero far from the torch:

$$E(z, 0) = 0, \qquad E(z, +\infty) = 0, \qquad E(\pm\infty, r) = 0 \tag{5}$$

The radiofrequency electromagnetic field generates small oscillating perturbations on all flowfield quantities. By averaging the flow equations in time, a quasi-steady flow formulation similar to the steady Navier–Stokes equations is obtained. In the momentum equation, a time-averaged Lorentz force $\boldsymbol{F}_L$ appears, whereas in the energy equation a time-averaged Joule heating source term P_J must be taken into account.

We simplify the flowfield description on the basis of the following considerations:

1) Because Reynolds numbers are low ($Re \sim 500$), we consider the flow to be laminar; hence no turbulence modeling terms need to be included.

2) Mach numbers are sufficiently low ($M < 0.3$) for the contribution of kinetic energy to the enthalpy and the power of the viscous stresses in the global energy equation to be neglected.

3) For the considered operating pressures (<1 atm), radiative effects may be neglected in air ICPs.[5]

This leads to the following set of flowfield equations:

1) continuity

$$\frac{\partial r\rho u}{\partial z} + \frac{\partial r\rho v}{\partial r} = 0 \tag{6}$$

2) z-momentum

$$\frac{\partial r(\rho u^2 + p)}{\partial z} + \frac{\partial r\rho uv}{\partial r} = \frac{\partial r\tau_{zz}}{\partial z} + \frac{\partial r\tau_{zr}}{\partial r} + rF_L^z \tag{7}$$

3) r-momentum

$$\frac{\partial r\rho uv}{\partial z} + \frac{\partial r(\rho v^2 + p)}{\partial r} = \frac{\partial r\tau_{zr}}{\partial z} + \frac{\partial r\tau_{rr}}{\partial r} + p + \rho w^2 - \tau_{\theta\theta} + rF_L^r \tag{8}$$

4) θ-momentum

$$\frac{\partial r\rho uw}{\partial z} + \frac{\partial r\rho vw}{\partial r} = \frac{\partial r\tau_{z\theta}}{\partial z} + \frac{\partial r\tau_{r\theta}}{\partial r} - \rho vw + \tau_{r\theta} \tag{9}$$

5) energy

$$\frac{\partial r\rho uh}{\partial z} + \frac{\partial r\rho vh}{\partial r} = \frac{\partial rq_z}{\partial z} + \frac{\partial rq_r}{\partial r} + rP_J \tag{10}$$

The shear stress components τ_{ij} take the form

$$\tau_{zz} = 2\mu\frac{\partial u}{\partial z} - \frac{2}{3}\mu\left(\frac{\partial u}{\partial z} + \frac{\partial v}{\partial r} + \frac{v}{r}\right)$$

$$\tau_{zr} = \tau_{rz} = \mu\left(\frac{\partial u}{\partial r} + \frac{\partial v}{\partial z}\right)$$

$$\tau_{rr} = 2\mu\frac{\partial v}{\partial r} - \frac{2}{3}\mu\left(\frac{\partial u}{\partial z} + \frac{\partial v}{\partial r} + \frac{v}{r}\right)$$

$$\tau_{z\theta} = \mu\frac{\partial w}{\partial z}, \qquad \tau_{r\theta} = \mu\left(\frac{\partial w}{\partial r} - \frac{w}{r}\right)$$

$$\tau_{\theta\theta} = -\frac{2}{3}\mu\left(\frac{\partial u}{\partial z} + \frac{\partial v}{\partial r} - 2\frac{v}{r}\right) \tag{11}$$

Indicating the components of the mass diffusion flux of species s by $\boldsymbol{J}_s = (J_s^z, J_s^r, J_s^\theta)$, the heat flux components are written

$$q_z = -\sum_{s=1}^{N_{sp}} J_s^z h_s + \lambda\frac{\partial T}{\partial z}, \qquad q_r = -\sum_{s=1}^{N_{sp}} J_s^r h_s + \lambda\frac{\partial T}{\partial r} \tag{12}$$

where $\lambda = \lambda_h + \lambda_e + \lambda_R + \lambda_V + \lambda_E$ accounts for all nonreactive[2] contributions to the thermal conductivity under thermal equilibrium (heavy particles, electron translational, rotational, vibrational, and electronic thermal conductivities).

Indicating the real and complex parts of the electric field amplitude by E_R and E_I, the time-averaged Lorentz forces F_L^z and F_L^r are written

$$F_L^z = \frac{\sigma}{4\pi f}\left(\frac{E_R}{r}\frac{\partial rE_I}{\partial z} - \frac{E_I}{r}\frac{\partial rE_R}{\partial z}\right)$$

$$F_L^r = \frac{\sigma}{4\pi f}\left(\frac{E_R}{r}\frac{\partial rE_I}{\partial r} - \frac{E_I}{r}\frac{\partial rE_R}{\partial r}\right) \tag{13}$$

The time-averaged Joule heating source term is given by

$$P_J = (\sigma/2)\left(E_R^2 + E_I^2\right) \tag{14}$$

Chemical Composition

Chemical Nonequilibrium (CNEQ)

Under chemical nonequilibrium conditions, the mixture composition is obtained from partial differential equations describing the advection, diffusion, and chemical processes that make the species concentrations vary within the torch. These equations read, for a species s:

$$\frac{\partial r\rho u y_s}{\partial z} + \frac{\partial\, r\rho v y_s}{\partial r} = -\frac{\partial r J_s^z}{\partial z} - \frac{\partial\, r J_s^r}{\partial r} + r\dot{\omega}_s \qquad (15)$$

Note that the index s runs over heavy particles only; we obtain the electron mole fraction by explicitly imposing quasi-neutrality:

$$x_e - \sum_{s\,\in\,\text{ions}} x_s = 0$$

For a given set of N_r chemical processes of the type

$$\sum_{s=1}^{N_{\text{sp}}} \nu'_{s,r} A_s \underset{k_{b,r}}{\overset{k_{f,r}}{\rightleftharpoons}} \sum_{s=1}^{N_{\text{sp}}} \nu''_{s,r} A_s$$

the mass production terms $\dot{\omega}_s$, present in the species continuity equations, are computed using the law of mass action,[25]

$$\dot{\omega}_s = \sum_{r=1}^{N_r} \omega_{sr} \qquad (16)$$

where

$$\omega_{sr} = M_s(\nu''_{s,r} - \nu'_{s,r}) k_{f,r} \left\{ \prod_{k=1}^{N_{\text{sp}}} \left(\frac{\rho_k}{M_k}\right)^{\nu'_{k,r}} - k_{b,r} \prod_{k=1}^{N_{\text{sp}}} \left(\frac{\rho_k}{M_k}\right)^{\nu''_{k,r}} \right\}$$

and $k_{b,r} = k_{f,r}/K_{c,r}$, $K_{c,r}$ being the equilibrium constant of reaction r computed from statistical mechanics.[25] All the computations presented in this paper under chemical nonequilibrium were performed using Park's model[26] for finite rate chemistry. Equations (15) describe a wide variety of physical phenomena and in particular allow for demixing of elements in the plasma [see Eq. (17)].

Chemical Equilibrium

It is well known[25] that the composition of a mixture of thermally perfect gases under thermochemical equilibrium can be obtained as a function of two independent thermodynamic variables for given fractions of elements in the mixture (e.g., oxygen and nitrogen for the air mixture considered here).

1) LTE, variable elemental fraction (LTE-VEF)

To correctly account for the fact that elemental fractions vary, one should solve a set of elemental continuity equations that can be obtained as a linear combination of the species continuity equations. Multiplying Eqs. (15) by $\phi_s^c M_c/M_s$ and summing over all species, one obtains:

$$\frac{\partial r\rho u Y_c}{\partial z} + \frac{\partial r\rho v Y_c}{\partial r} = -\frac{\partial r \mathcal{J}_c^z}{\partial z} - \frac{\partial r \mathcal{J}_c^r}{\partial r} \qquad (17)$$

where the index c runs over the N_{el} elements contained in each species of the mixture (N and O in the present case). The previous set of equations, valid regardless of the degree of chemical nonequilibrium, can be solved with respect to the element mass fractions Y_c, defined as

$$Y_c = \sum_{s=1}^{N_{\text{sp}}} \phi_s^c y_s \frac{M_c}{M_s} \qquad (18)$$

From an analysis of Eq. (17) one clearly observes that diffusion of species results in elemental diffusion by means of element mass diffusion fluxes that take the form

$$\mathcal{J}_c = \sum_{s=1}^{N_{\text{sp}}} \phi_s^c \boldsymbol{J}_s \frac{M_c}{M_s} \qquad (19)$$

This will in general induce variations of elemental concentrations inside a plasma torch even when the elemental composition of the injected gas mixture is uniform. It is interesting to notice that this phenomenon is independent of the degree of chemical nonequilibrium[15,27] owing to the absence of chemical source terms in Eqs. (17). In Ref. 18 an alternative form of Eq. (19) is proposed, where the elemental mass diffusion fluxes are expressed as linear combination of temperature and elemental mass fraction gradients at constant pressure and under thermochemical equilibrium conditions. Following this approach, Eqs. (19) for oxygen and nitrogen read

$$\mathcal{J}_O = -\rho D_O^T \nabla T - \rho D_O^{\text{Tot}} \nabla Y_O \qquad (20a)$$

$$\mathcal{J}_N = -\rho D_N^T \nabla T - \rho D_N^{\text{Tot}} \nabla Y_N \qquad (20b)$$

Detailed expressions for the elemental thermal demixing and elemental diffusion coefficients D_c^T and D_c^{Tot} are given in Ref. 18. Because under thermochemical equilibrium and at constant pressure

$$\nabla x_s = \left.\frac{\partial x_s}{\partial T}\right|_{Y_f,p} \nabla T + \sum_{f\,=\,1,\ldots,N_{\text{el}}} \left.\frac{\partial x_s}{\partial Y_f}\right|_{T,p} \nabla Y_f$$

the thermal demixing diffusion coefficients are proportional to

$$\left.\frac{\partial x_s}{\partial T}\right|_{Y_f,p}$$

whereas the total mixing diffusion coefficients depend linearly on

$$\left.\frac{\partial x_s}{\partial Y_f}\right|_{T,p}$$

These observations will be helpful in the following section to justify the boundary condition used on solid surfaces for Eq. (17).

We now focus on chemical equilibrium conditions. For a set of N_{sp} species among which N_{ic} independent and N_r dependent components can be identified, the mixture composition can be found as the solution of the following nonlinear system[28,29]:

$$\sum_{s=1}^{N_{\text{sp}}} \nu_s^r \ell_n x_s = \ell_n K_x^r \qquad (r = 1, \ldots, N_r) \qquad (21)$$

$$\sum_{s=1}^{N_{\text{sp}}} \phi_s^c x_s = X_c \frac{\bar{n}}{n} \qquad (c = 1, \ldots, N_{\text{ic}}) \qquad (22)$$

$$\sum_{s=1}^{N_{\text{sp}}} x_s = 1 \qquad (23)$$

where ν_s^r are the stoichiometric coefficients normalized such that $\nu_r^r = 1$, K_x^r is the equilibrium constant for reaction r based on species mole fractions,[25] n and $\bar{n}$ are the total number densities of respectively all species and all elements,[28,30] and X_c is the volumetric fraction of element c, given by

$$X_c = \frac{Y_c/M_c}{\sum_{i=1}^{N_{\text{el}}} Y_i/M_i} \qquad (24)$$

As an example, for the 11-species mixture defined at the beginning of the paper we identify 8 dependent components $\left(\text{N}_2, \text{O}_2, \text{NO}, \text{NO}^+, \text{O}^+, \text{N}^+, \text{O}_2^+, \text{N}_2^+\right)$ and 3 elements (oxygen and nitrogen plus the mixture charge). The mass fraction of charge is set to zero everywhere, in line with the quasi-neutrality assumption. Hence only demixing of 2 elements (O, N) needs to be considered in the end.

The solution of the system (21–23) provides the species mole fractions x_s as a function of temperature (T), pressure (p), and elemental mass fractions (Y_c). In each cell of the computational domain,

temperature and pressure are found as the solution of respective the energy and global continuity equation, while the elemental mass fractions follow from the elemental continuity equations (17).

2) LTE, constant elemental fraction (LTE-CEF)

If elemental diffusion is neglected, then the mixture composition is determined from Eqs. (21–23) assuming elemental fractions to be constant in the flowfield, equal to their inlet values. For this particular case, the condition $\mathcal{J}_c = 0$ corresponding to vanishing elemental fluxes[2] and conduction current[30] allows for the diffusive transport of enthalpy to be reduced to the Fourier-type heat flux term shown in Eq. (1),[30] where λ_r^{BB} is the thermal reactive conductivity.

Flow and Composition Boundary Conditions

We refer to ambient conditions using the index A.

Axis of Symmetry

At the torch axis, we impose symmetry:

$$\frac{\partial p}{\partial r} = 0, \qquad \frac{\partial \rho u}{\partial r} = 0, \qquad \rho v = 0, \qquad \frac{\partial \rho w}{\partial r} = 0, \qquad \frac{\partial T}{\partial r} = 0$$

$$\text{CNEQ: } \frac{\partial x_s}{\partial r} = 0, \qquad \text{LTE-VEF: } \frac{\partial Y_c}{\partial r} = 0$$

Torch Outlet

We take the torch outlet corresponding to a discharge in ambient space:

$$p = p_{\mathrm{A}}, \qquad \frac{\partial \rho \boldsymbol{u}}{\partial z} = 0, \qquad \frac{\partial T}{\partial z} = 0$$

$$\text{CNEQ: } \frac{\partial x_s}{\partial z} = 0, \qquad \text{LTE-VEF: } \frac{\partial Y_c}{\partial z} = 0$$

where p_{A} stands for the ambient pressure in the outlet vessel.

Quartz Tube Wall

On the quartz tube inner surface, no-slip boundary conditions are imposed:

$$\frac{\partial p}{\partial r} = 0, \qquad \rho \boldsymbol{u} = 0, \qquad T = T_{\mathrm{wall}}$$

The species concentrations are extrapolated by imposing homogeneous Neumann boundary conditions corresponding to a noncatalytic surface:

$$\text{CNEQ} : \frac{\partial x_s}{\partial r} = 0 \tag{25}$$

When the variable elemental fraction LTE model is used, we use the following boundary condition instead:

$$\text{LTE-VEF: } \frac{\partial Y_c}{\partial r} = 0 \tag{26}$$

The reader may remark that the conditions (25) and (26) are not necessarily equivalent when LTE conditions are reached. The mole fractions depend not only on the elemental concentrations but also on temperature (and to a lesser extent, pressure). Therefore, if a temperature gradient exists, nonzero mole fraction gradients may be obtained even when gradients of elemental fractions vanish. In high-pressure ICPs, however, temperatures near the wall ~300 K are too low to cause chemical reactions. Within this low-temperature zone (where $\partial x_s / \partial T|_{Y_f, p} = 0$), gradients of temperature do not induce concentration gradients such that the boundary conditions (25) and (26) become fully equivalent in the LTE limit.

Torch Inlet

The flow is injected through a thin ring near the torch wall. The axial inlet momentum Q is to be calculated from a given total mass injection rate. The model allows for an azimuthal inlet momentum component, which is taken to be a "swirl" number S times the axial inlet momentum. This translates into the following inlet boundary condition:

$$\frac{\partial p}{\partial z} = 0, \qquad \rho u = Q, \qquad \rho v = 0, \qquad \rho w = S \times Q, \qquad T = T_{\mathrm{A}}$$

$$\text{CNEQ: } x_s = x_{\mathrm{A},s}, \qquad \text{LTE-VEF: } Y_c = Y_{\mathrm{A},c}$$

where the temperature, the composition, and the elemental concentrations of the (cold) ambient gas fed to the torch are written, respectively, T_{A}, $x_{\mathrm{A},s}$, and $Y_{\mathrm{A},c}$.

In the ICP torches for TPS material testing simulated here, the central inlet is generally removed and replaced by a solid wall (see Fig.1); there, we impose an adiabatic no-slip condition:

$$\frac{\partial p}{\partial z} = 0, \qquad \rho \boldsymbol{u} = 0, \qquad \frac{\partial T}{\partial z} = 0$$

$$\text{CNEQ: } \frac{\partial x_s}{\partial z} = 0, \qquad \text{LTE-VEF: } \frac{\partial Y_c}{\partial z} = 0$$

Observe that in this case the boundary condition $\partial Y_c / \partial z = 0$ is valid, not because the temperature is low, but because the temperature gradient $\partial T / \partial z = 0$.

Thermodynamic and Transport Properties

A detailed overview of the thermodynamic and transport property models used has been given in previous works on LTE air plasmas[5,30–32] and here we only briefly recapitulate the main ideas of these studies.

The species selected to simulate the air mixture possess discrete rotational, vibrational, and (or) electronic internal energies.[25] Bottin et al.[30] have shown that, for temperatures up to ~10,000 K typical of high-pressure ICPs, these internal degrees of freedom may be treated in a decoupled manner by assuming that molecules rotate in a rigid manner and oscillate harmonically, independent of their electronic state.

Only a finite number of electronic modes need to be taken into account; the precise number differs from species to species as given in Ref. 30. Vibrational and rotational constants are taken for the ground electronic state. The species and mixture transport properties are obtained with the method of Chapman and Enskog.[17] The viscosity μ and heavy particle thermal conductivity λ_h are computed with the mixture rules of Yos,[33] as listed by Gupta et al.[21] The rotational, vibrational, and electronic thermal conductivities λ_R, λ_V, and λ_e are modeled by means of the Eucken approximation.[21] The electron thermal conductivity λ_E and electrical conductivity σ are computed with the formulas due to Devoto,[34] where two nonvanishing Sonine polynomial contributions were found to yield accurate results.[30] Special care has been devoted to the computation of the mass diffusion fluxes $\boldsymbol{J}_s$. In the present computational model, diffusion fluxes are evaluated using the full Stefan–Maxwell equations, which are mathematically equivalent to the Chapman–Enskog multicomponent diffusion expressions.[35] Neglecting pressure and thermal diffusion as well as the effect of the magnetic field,[5] we have

$$\frac{M}{\rho} \sum_{t=1}^{N_{\mathrm{sp}}} \left(\frac{x_s M_s \boldsymbol{J}_t - x_t M_t \boldsymbol{J}_s}{M_s M_t \mathcal{D}_{st}} \right) = \nabla x_s - \frac{\rho y_s \mathcal{Q}_s}{p} \boldsymbol{E}_{\mathrm{amb}} \tag{27}$$

where M_s are the species molar masses, M is the mixture molar mass, x_s are the molar fractions, and $\mathcal{Q}_s$ is the species charge per unit mass. The binary diffusion coefficients $\mathcal{D}_{\mathrm{st}}$ can be further expressed as

$$\mathcal{D}_{\mathrm{st}} = \frac{3}{16 n} \sqrt{\frac{2\pi k_B T}{m_{\mathrm{st}}}} \frac{1}{\bar{\Omega}_{\mathrm{st}}^{11}} \tag{28}$$

where k_B is Boltzmann's constant and the reduced mass of the particle pair st is written as $m_{st} = m_s m_t/(m_s + m_t)$ (in kg). Readers eager to reproduce the results obtained in this paper may find detailed curve fits for the collision integrals of air mixtures in Ref. 30.

As said, we assume that no net electric current flows in the poloidal (r, z) plane under conditions of LTE.[5] The ambipolar electric field $\boldsymbol{E}_{\text{amb}}$ is then determined by imposing the additional constraint that

$$\sum_{s=1}^{N_{\text{sp}}} \mathcal{Q}_s \boldsymbol{J}_s = 0 \tag{29}$$

Equations (27–29) represent a linear system (one in each coordinate direction) in $N_{\text{sp}} + 1$ unknowns, the diffusion fluxes and the ambipolar electric field, which are solved using an iterative method proposed in Ref. 36, adapted to the case of diffusion in ionized mixtures.

Different physics takes place in the azimuthal direction, where strong electric currents act. Diffusion is driven by the azimuthal induced electric field [Eq. (3)] instead of the poloidal ambipolar field [Eqs. (29) and (27)] can be reduced to Ohm's law in its simplest form,

$$\mathcal{Q}_e \boldsymbol{J}_e = \sigma \boldsymbol{E} \tag{30}$$

which has been used to derive Eq. (4). More details about the numerical method used to solve the previous system of equations can be found in Refs. 5 and 37.

Numerical Results

We will now present and analyze numerical results for air ICPs inside the VKI Plasmatron torch (Fig. 1), obtained using 1) the full chemical nonequilibrium formulation (CNEQ), 2) the consistent LTE formulation that allows for varying element fractions (LTE-VEF), and 3) the simplified LTE model (LTE-CEF) assuming a fixed elemental volumetric composition (21% oxygen, 79% nitrogen). In our numerical model, both the electromagnetic and flowfield equations are discretized by means of a second-order accurate collocated finite volume method on a structured mesh of 131 by 47 cells. To assess the degree of grid convergence, for a reference set of operating conditions, additional computations have been performed on a mesh of 262 by 94 cells and the differences in the results were found to be below 2–3%.

The discretized equations are solved using a damped Newton method where the GMRES algorithm with BILU(0)[38] preconditioning is used as a linear solver.[5] All results presented in this paper are converged to at least six orders of magnitude (based on the drop in the L_2 residual norm). The qualitative analysis of the obtained results will be based upon comparison of computed contour plots. To perform an accurate quantitative analysis, we will also present plots of radial variations of flow quantities in the plasma, obtained close to the inlet ($z = 0.056$ m), at the midcoil position ($z = 0.265$ m), and at the outlet ($z = 0.486$ m), as indicated in Fig. 2a. The operating conditions used for the simulations are listed in Table 1.

Flowfield and Concentration Analysis

In Figs. 2a–2c, we compare temperature, flowfield, and volumetric oxygen fraction contours computed at a pressure of 0.05 atm using the CNEQ and the LTE-VEF formulations. Inspection of the temperature fields shows that chemical nonequilibrium effects have an important influence at this relatively low operating pressure.

Table 1 Plasmatron operating conditions

Ambient and wall temperature, K	300
Power injected into the plasma, kW	75
Frequency, MHz	0.45
Inlet swirl, deg	45
Mass flow, g/s	6
Operating pressures, atm	0.05, 0.1, 0.2, 0.3

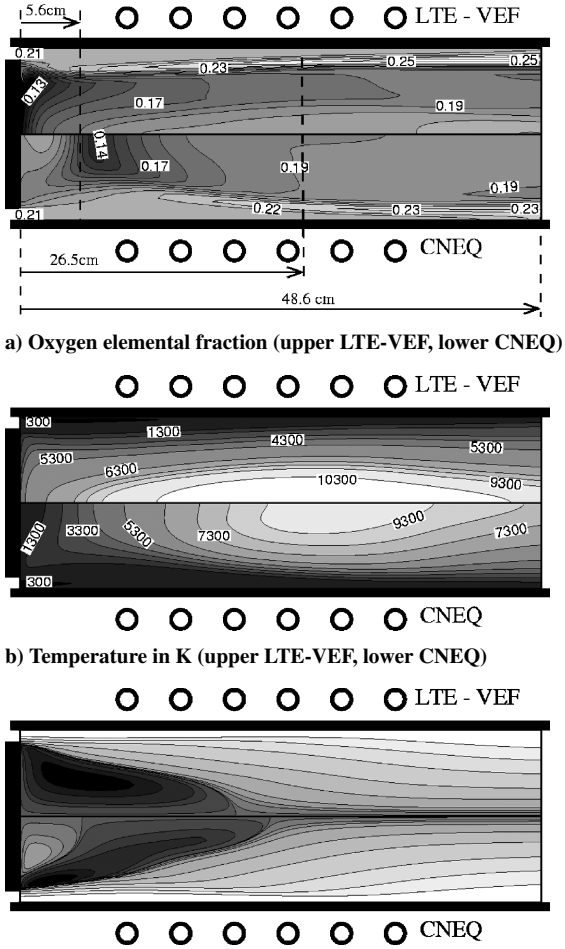

Fig. 2 Computed oxygen elemental fraction, temperature, and stream function in an air ICP torch at an ambient pressure of 0.05 atm.

Because of the lower temperatures found in the CNEQ case, viscosity is smaller, the Reynolds number is higher and a small secondary recirculation appears near the inlet. Both the CNEQ and the LTE-VEF computations show that variations of oxygen elemental fractions are significant. The fact that variations are of similar order of magnitude for both formulations indicates that elemental demixing in chemically reacting thermal plasma flows is not a CNEQ effect. The reason for this is, of course, that no chemistry terms appear in the elemental continuity Eqs. (17). Due to the strong temperature gradients in the radial direction, concentration variations and diffusion also mainly act perpendicular to the wall. Because the atomic oxygen contained inside the plasma ball diffuses faster than the (heavier) molecular oxygen in the low-temperature zones adjacent to the wall, we observe a strong increase in the overall fraction of oxygen elements near the wall. Strong depletion of oxygen is observed on the axis at the outlet and also in the recirculation bubble near the inlet, where the flow particles have a larger residence time. When TPS material tests are performed using high-pressure air ICPs, the outlet conditions of our torch simulations correspond to inlet conditions for a jet of hot plasma flowing into a test chamber and impacting on a TPS sample. We expect that the oxygen depletion process due to demixing will continue inside the test chamber. Hence the elemental composition of the air mixture hitting the TPS is likely to be far from the 21% oxygen/79% nitrogen composition commonly assumed by researchers performing TPS tests. It therefore appears to be desirable to take into account the demixing effect in the TPS testing methodology in the future. In particular, to quantitatively assess the importance of elemental demixing on TPS catalycity activity, a further investigation of demixing in the jet leaving the torch and impacting on the TPS sample should be performed.

Parametric Study of the Influence of Pressure

In this section we present results for all operating pressures specified in Table 1 to provide (1) a thorough comparison between the LTE-CEF and LTE-VEF formulations and (2) to show that the LTE-VEF formulation is as accurate as the CNEQ model for sufficiently high pressures.

In Fig. 3, we present radial profiles of volumetric oxygen fraction and temperature obtained in the inlet zone ($z = 0.056$ m). For a pressure of 0.05 atm, comparison of the temperature profiles shows that nonequilibrium effects are quite high in the inlet zone, where temperatures are low. Differences in terms of temperature profiles between the LTE-CEF and LTE-VEF formulations are very low above 3 cm, whereas they increase up to a maximum of around 1000 K on the axis. The oxygen element profiles obtained using the CNEQ and the LTE-VEF formulations show a clear peak at $r \approx 6.5$ cm, while using the LTE-CEF formulation obviously the oxygen fraction is constant. As pressure is increased, the influence of demixing on temperature decreases and the results obtained with the LTE-CEF and LTE-VEF formulations tend to converge. A similar tendency is obtained for the radial profile under CNEQ, which starts far from the two corresponding to LTE-CEF and LTE-VEF at 0.05 atm and approaches the LTE results at higher pressure. For the highest pressure (Fig. 3h) some differences are present and confined to a small region around the axis (here for $r \leq 2$ cm). The analysis of the oxygen profiles shows that both the CNEQ and the LTE-VEF formulations predict the same order of magnitude for oxygen elemental diffusion; the LTE-CEF model does not provide this information.

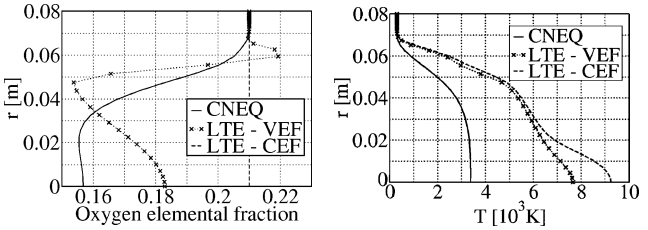

a) $X_O(r)$ at 0.05 atm b) $T(r)$ at 0.05 atm

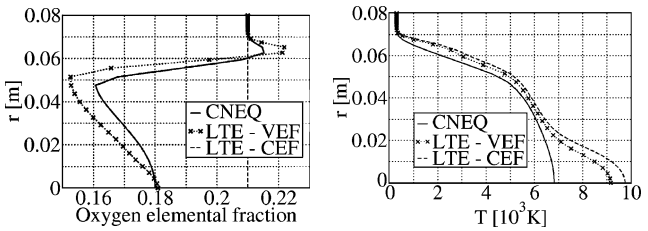

c) $X_O(r)$ at 0.1 atm d) $T(r)$ at 0.1 atm

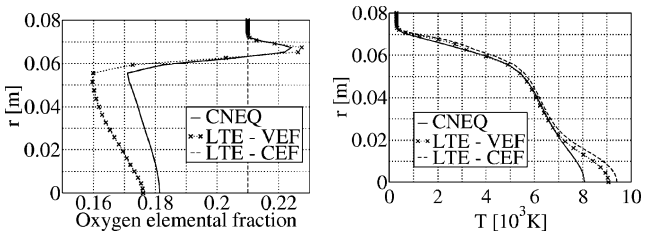

e) $X_O(r)$ at 0.2 atm f) $T(r)$ at 0.2 atm

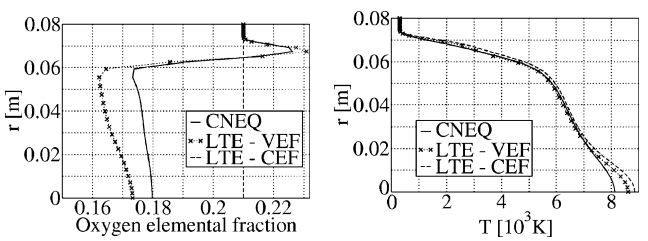

g) $X_O(r)$ at 0.3 atm h) $T(r)$ at 0.3 atm

Fig. 3 Oxygen elemental fraction and temperature profiles for several operating pressures at $z = 0.056$ m.

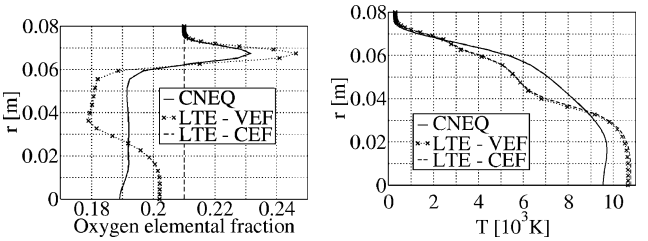

a) $X_O(r)$ at 0.05 atm b) $T(r)$ at 0.05 atm

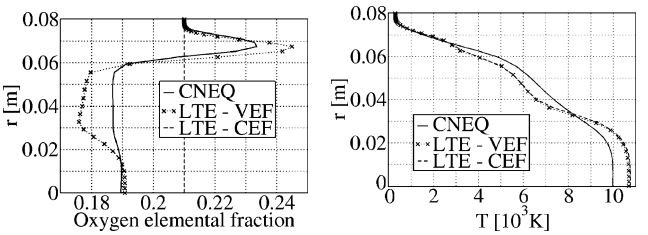

c) $X_O(r)$ at 0.1 atm d) $T(r)$ at 0.1 atm

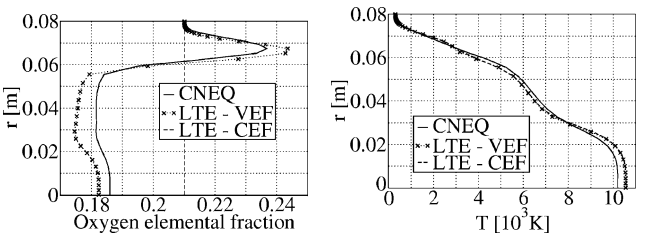

e) $X_O(r)$ at 0.2 atm f) $T(r)$ at 0.2 atm

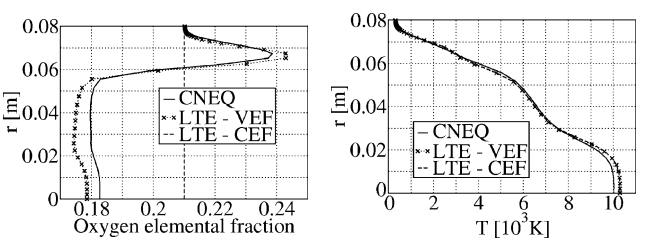

g) $X_O(r)$ at 0.3 atm h) $T(r)$ at 0.3 atm

Fig. 4 Oxygen elemental fraction and temperature profiles for several operating pressures at $z = 0.265$ m.

In Fig. 4 we focus on the mid-coil zone ($z = 0.265$ m). All oxygen elemental fraction profiles start from a value of 0.21 at the quartz tube, as in the previous position (Fig. 3), showing that demixing is prevalent in the radial direction. Indeed the cold zone close to the quartz tube is characterized by a mainly constant oxygen concentration, where the flow is continuously filled by an annular jet of O_2/N_2 in the molar ratio of 21/79. All the profiles corresponding to the CNEQ formulation present a peak at the edge of the plasma ball (here for $r \approx 6.5$ cm) and then become flat at lower radii. Again we observe that the oxygen profiles obtained under LTE-VEF and CNEQ reasonably match for $p \geq 0.2$ atm. The analysis of temperature profiles show that, at the midcoil section, the influence of elemental demixing on the temperature prediction is negligible. Indeed the temperature profiles obtained with the LTE-CEF and LTE-VEF formulations are superposed for all pressures and all radii. In addition the differences with respect to the CNEQ results decreases as pressure is increased, as expected.

In Fig. 5, we compare computed profiles of temperature and oxygen element fraction obtained at the outlet of the torch ($z = 0.486$ m). The general evolution of the oxygen elemental fraction follows the description presented for the midcoil section. Some small differences are visible close to the quartz tube. Indeed we observe that the LTE-VEF and the CNEQ oxygen profiles start from a value slightly higher than 0.21 showing that demixing has the tendency to enrich the cold flow region in oxygen (element) and that some axial diffusion takes place near the outlet. From the analysis of the

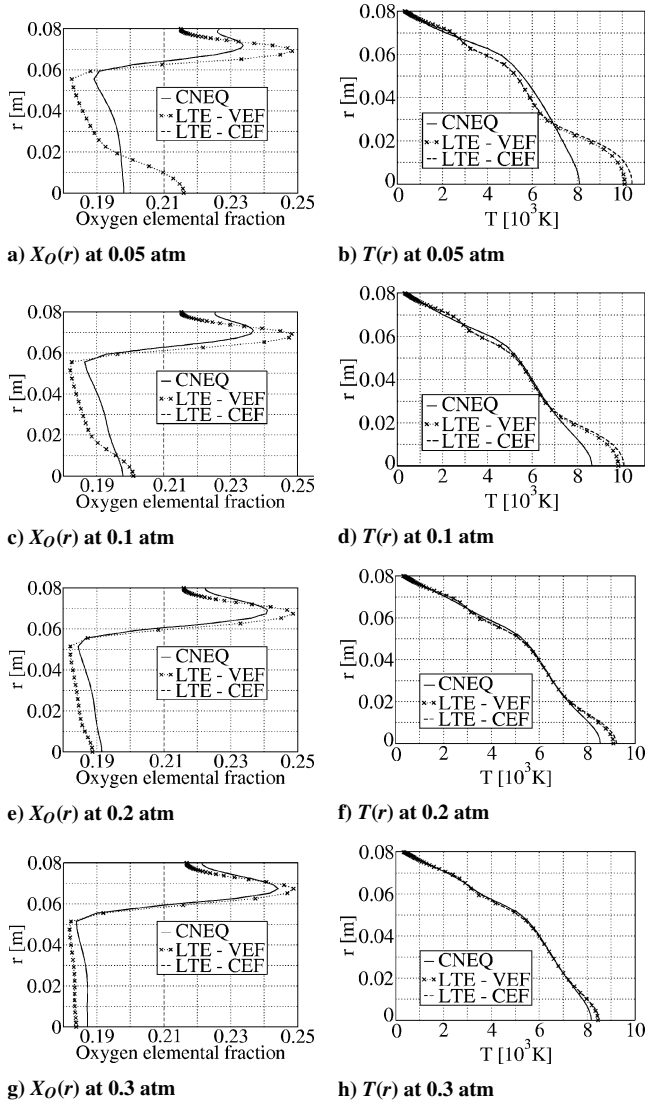

a) $X_O(r)$ at 0.05 atm b) $T(r)$ at 0.05 atm

c) $X_O(r)$ at 0.1 atm d) $T(r)$ at 0.1 atm

e) $X_O(r)$ at 0.2 atm f) $T(r)$ at 0.2 atm

g) $X_O(r)$ at 0.3 atm h) $T(r)$ at 0.3 atm

Fig. 5 Torch outlet profiles ($z = 0.486$ m) of oxygen elemental fraction and temperature for increasing ambient pressures.

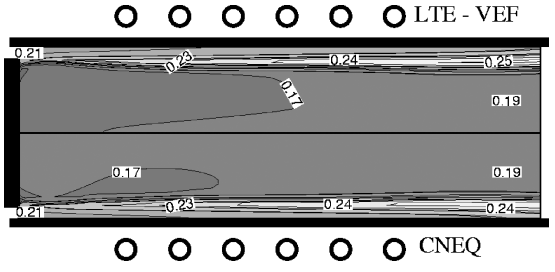

Fig. 6 Elemental fraction in the torch at 0.3 atm (upper LTE-VEF, lower CNEQ).

temperature profiles, we observe that elemental demixing slightly affects the temperature profiles only at low pressures. Therefore for what concerns the determination of TPS catalycity properties the only influence that demixing could have, for Earth entry applications and for sufficiently high pressures, is related to different elemental and species concentration at the inlet of the chamber.

Another conclusion, important from both modeling and physical points of view, could be drawn from Fig. 5. Indeed, as the ambient pressure increases, the CNEQ results clearly start to approach the LTE-VEF results, which is to be expected as chemistry becomes faster at higher pressures. Therefore the inlet conditions for the test chamber can be accurately computed with an LTE-VEF formulation for sufficiently high pressures. This is also supported by the contour plot of oxygen nuclei fraction at 0.3 atm shown in Fig. 6: differences are quite small in agreement with Figs. 3–4 and especially if compared with the same plot at 0.05 atm (Fig. 2).

In the remaining part of this section we discuss the effects of elemental demixing on the species profiles at the torch outlet for the 0.3 atm operating pressure. In Fig. 7 we compare the outlet mole fraction profiles at 0.3 atm for three physical formulations. We clearly see that differences between the CNEQ and the LTE-CEF formulations, at higher pressures, are mainly due to elemental diffusion effects, rather than chemistry. This conclusion is useful for the modeling of plasma torches. Indeed, in view of this result, for sufficiently high pressures, we can avoid the solution of a set of N_{sp} species equations [Eqs. (15)], with stiff source terms, in favor of a lighter, more elegant and reliable model containing only N_{el} equations (two in the present case) without source terms. A further reduction of the small discrepancies present at the torch outlet at 0.3 atm is possible by acting directly on the chemistry characteristic time under nonequilibrium conditions. If we artificially increases the reaction rates in the CNEQ simulations at 0.3 atm, by multiplying $\dot{\omega}_s$ by a factor 10^3 in Eqs. (15), then differences become tiny, as can be seen in Figs. 8, 9, and 10. This clearly shows that the CNEQ regime tends to the

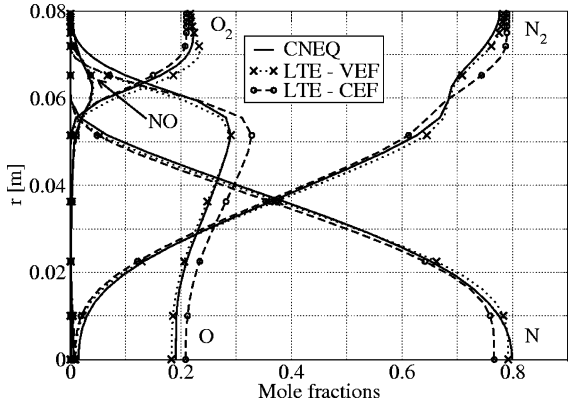

Fig. 7 Outlet species mole fraction profiles ($z = 0.486$ m) at 0.3 atm.

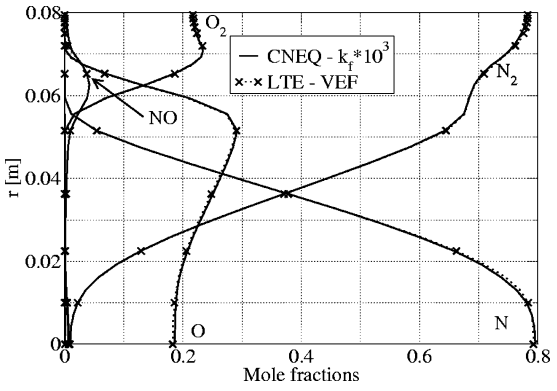

Fig. 8 Outlet species mole fractions ($z = 0.486$ m) at 0.3 atm ($10^3 \times \dot{\omega}_s$).

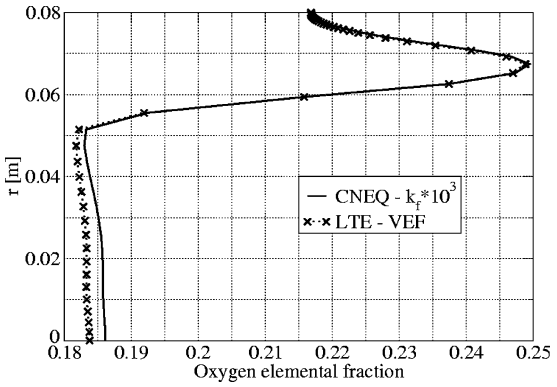

Fig. 9 Outlet elemental fraction profiles ($z = 0.486$ m) at 0.3 atm ($10^3 \times \dot{\omega}_s$).

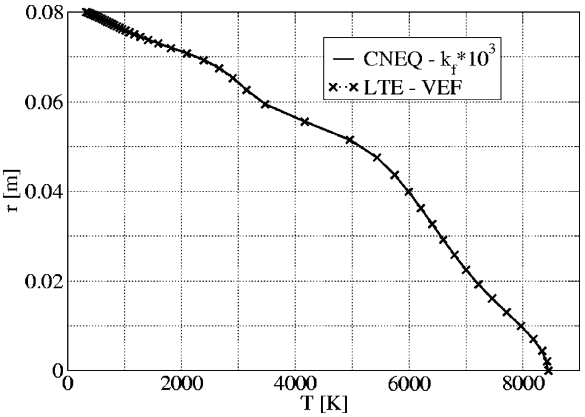

Fig. 10 Outlet temperature profile ($z = 0.486$ m) at 0.3 atm ($10^3 \times \dot{\omega}_s$).

LTE-VEF regime as the speed of chemistry increases as observed in Ref. 15 for stagnation line flows.

Conclusions

In this paper, we have proposed an LTE formulation of the equations of reacting flows of partially ionized mixtures, which allows for variations in the concentrations of chemical elements due to diffusion. We have applied this formulation to simulate an existing high-pressure air inductively coupled plasma torch operating at pressures ranging from 0.05 to 0.3 atm. An analysis of these results and a comparison with corresponding results obtained under chemical nonequilibrium leads us to the following conclusions:

1) In high-pressure ICP torches, the oxygen concentration varies significantly throughout the flowfield. From the large series of calculation presented, we find that for an inlet volumetric oxygen fraction of 21%,

a) The oxygen content typically decreases to ∼15% inside the recirculation near the inlet and to ∼17–18% at the outlet, on the axis.

b) At the edges of the plasma ball, closer to the quartz wall, the oxygen content typically reaches ∼25%.

c) On the quartz wall, due to convection from the inlet, the oxygen content remain close to ∼21%.

2) While it significantly affects the plasma concentration, the effect of demixing on obtained temperature fields is very low, at least for the case of air ICPs. In order to quantitatively asses the influence of elemental demixing on the determination of TPS catalytic properties we therefore suggest to extend the present study to the hot jet exiting the torch.

3) Demixing occurs regardless of the degree of chemical nonequilibrium in the plasma. At sufficiently high pressures (0.3 atm for the torch considered here), the local thermodynamic equilibrium formulation with variable elemental fraction is as accurate as the chemical nonequilibrium formulation.

4) Chemical equilibrium conditions do exist in viscous flows at sufficiently high pressures and chemical reaction terms based upon the law of mass action are compatible with this fact.

References

[1]Sarma, G. S. R., "Physico-chemical Modeling in Hypersonic Flow Simulation," *Progress in Aerospace Sciences*, Vol. 36, No. 3–4, 2000, pp. 281–349.

[2]Butler, J. N., and Brokaw, R. S., "Thermal Conductivity of Gas Mixtures in Chemical Equilibrium," *Journal of Chemical Physics*, Vol. 26, No. 6, 1957, pp. 1636–1643.

[3]Brokaw, R. S., "Thermal Conductivity of Gas Mixtures in Chemical Equilibrium, II," *Journal of Chemical Physics*, Vol. 32, No. 4, 1960, pp. 1005, 1006.

[4]Vasil'evskii, S. A., Kolesnikov, A. F., and Yakushin, M. I., "Mathematical Models for Plasma and Gas Flows in Induction Plasmatrons," *Molecular Physics and Hypersonic Flows*, edited by M. Capitelli, Kluwer, Dordrecht, 1996, pp. 495–504.

[5]Vanden Abeele, D., and Degrez, G., "Efficient Computational Model for Inductive Plasma Flows," *AIAA Journal*, Vol. 38, No. 2, 2000, pp. 234–242.

[6]Magin, T., and Degrez, G., "Cooled Pitot Probe in Inductive Air Plasma Jet: What Do We Measure?" *2nd International Symposium on Atmospheric Reentry Vehicles and Systems*, Arcachon, France, March 2001.

[7]Suslov, O. N., Tirsky, G. A., and Shchennikov, V. V., "Flows of Multicomponent Ionized Mixtures in Chemical Equilibrium. Description Within the Framework of the Navier–Stokes and Prandtl Equations," *Prikladnaya Mekhanika i Teknicheskaya Fizika*, 1971, pp. 73–90.

[8]Tirsky, G. A., "Up-to-Date Gasdynamic Models of Hypersonic Aerodynamics and Heat Transfer with Real Gas Properties," *Annual Review of Fluid Mechanics*, Vol. 25, Jan. 1993, pp. 151–181.

[9]Tirsky, G. A., "The Hydrodynamic Equations for Chemically Equilibrium Flows of a Multielement Plasma with Exact Transport Coefficients," *Journal of Applied Mathematics and Mechanics*, Vol. 63, No. 6, 1999, pp. 841–861.

[10]Murphy, A. B., "Combined Diffusion Coefficients in Equilibrium Mixtures of Dissociating Gases," *Journal of Chemical Physics*, Vol. 99, No. 2, 1993, pp. 1340–1343.

[11]Murphy, A. B., "Diffusion in Equilibrium Mixtures of Ionized Gases," *Physical Review E*, Vol. 48, No. 5, 1993, pp. 3594–3603.

[12]Murphy, A. B., "Demixing Due to Frictional Forces in an Electric Arc," *Physical Review Letters*, Vol. 73, No. 13, 1994, pp. 1797–1800.

[13]Murphy, A. B., "Demixing in Free-Burning Arcs," *Physical Review E*, Vol. 55, No. 6, 1997, pp. 7473–7494.

[14]Van der Heijden, H. W. P., "Modeling of Radiative Transfer in Light Sources," Ph.D. Thesis, Technische Universiteit Eindhoven, Eindhoven, Jan. 2003.

[15]Rini, P., and Degrez, G., "Elemental Demixing in Air and Carbon Dioxide Stagnation Line Flows," *Journal of Thermophysics and Heat Transfer*, Vol. 18, No. 4, 2004, pp. 511–518; also AIAA Paper 2004-4261.

[16]Ferziger, J. H., and Kaper, H. G., *Mathematical Theory of Transport Processes in Gases*, North-Holland, Amsterdam, 1972.

[17]Hirschfelder, J. O., Curtiss, C. F., and Bird, R. B., *Molecular Theory of Gases and Liquids*, Wiley, New York, 1964.

[18]Rini, P., Vanden Abeele, D., and Degrez, G., "Closed Form for the Equations of Chemically Reacting Flows Under Local Thermodynamic Equilibrium," *Physical Review E*, Vol. 72, URL: http://link.aps.org/abstract/PRE/v72/e011204 [cited 22 July 2005].

[19]Bukowski, J. D., Graves, D. B., and Vitello, P., "Two-Dimensional Model of an Inductively Coupled Plasma with Comparison to Experimental Spatial Profiles," *Journal of Applied Physics*, Vol. 80, No. 5, 1996, pp. 2614–2623.

[20]Kolesnikov, A. F., "Extrapolation from High Enthalpy Tests to Flight Based on the Concept of Local Heat Transfer Simulation," NATO RTO-EN 8, von Karman Institute for Fluid Dynamics, St.-Genesius-Rode, Belgium, Oct. 1999.

[21]Gupta, R. N., Yos, J. M., Thompson, R. A., and Lee, K. P., "A Review of Reaction Rates and Thermodynamic and Transport Properties for an 11-Species Air Model for Chemical and Thermal Non-equilibrium Calculations to 30,000 K," NASA, Reference Publication 1232, Aug. 1990.

[22]Mitchner, M., and Kruger, C., *Partially Ionized Gases*, Wiley, New York, 1973.

[23]Jaeger, E. F., Berry, L. A., Tolliver, J. S., and Batchelor, D. B., "Power Deposition in High-Density Inductively Coupled Plasma Tools for Semiconductor Processing," *Physics of Plasmas*, Vol. 2, No. 6, 1995, pp. 2597–2604.

[24]Mekideche, M. R., "Contribution à la modélisation numérique de torches à plasma d'induction," Ph.D. Thesis, École Doctorale Sciences pour l'Ingénieur de Nantes, St. Nazaire, France, Oct. 1993.

[25]Vincenti, W., and Kruger, C., *Introduction to Physical Gas Dynamics*, Wiley, New York, 1965.

[26]Park, C., "Problems of Rate Chemistry in the Flight Regimes of Aeroassisted Orbital Transfer Vehicles," AIAA Technical Paper 84-1730, June 1984.

[27]Rini, P., Garcia, A., Magin, T., and Degrez, G., "Numerical Simulation of CO_2 Stagnation Line Flows with Catalyzed Surface Reactions," *Journal of Thermophysics and Heat Transfer*, Vol. 14, No. 1, 2004, pp. 114–121; also AIAA Paper 2003-4038.

[28]Magin, T., "A Model for Inductive Plasma Wind Tunnels," Ph.D. Thesis, von Karman Institute for Fluid Dynamics, St.-Genesius-Rode, Belgium, June 2004.

[29]Magin, T., and Degrez, G., "Transport Algorithms for Partially Ionized and Unmagnetized Plasmas," *Journal of Computational Physics*, Vol. 198, No. 2, 2004, pp. 424–449.

[30]Bottin, B., Vanden Abeele, D., Carbonaro, M., Degrez, G., and Sarma, G. S. R., "Thermodynamic and Transport Properties for Inductive Plasma Modeling," *Journal of Thermophysics and Heat Transfer*, Vol. 13, No. 3, 1999, pp. 343–350.

[31]Barbante, P. F., "Accurate and Efficient Modeling of High Temperature Nonequilibrium Air Flows," Ph.D. Thesis, von Karman Institute, Rhode-Saint-Genèse, Belgium, 2001.

[32]Barbante, P. F., and Magin, T., "Computation of Nonequilibrium High-Temperature Axisymmetric Boundary-Layer Flows," *Journal of Thermophysics and Heat Transfer*, Vol. 16, No. 4, 2004, pp. 490–497.

[33]Yos, J. M., "Approximate Equations for the Viscosity and Translational Thermal Conductivity of Gas Mixtures," Contract Report AVSSD-0112-67-RM, Avco Corporation, Wilmington, MA, April 1967.

[34]Devoto, R. S., "Simplified Expressions for the Transport Properties of Ionized Monoatomic Gases," *Physics of Fluids*, Vol. 10, No. 10, 1967, pp. 2105–2112.

[35]Hirschfelder, J. O., Curtiss, C. F., and Bird, R. B., *Molecular Theory of Gases and Liquids*, Wiley, New York, 1954.

[36]Sutton, K., and Gnoffo, P. A., "Multi-component Diffusion with Application to Computational Aerothermodynamics," Technical Paper 98-2575, AIAA, Albuquerque, NM, June 1998.

[37]Degrez, G., Vanden Abeele, D., Barbante, P., and Bottin, B., "Numerical Simulation of Inductively Coupled Plasma Flows Under Chemical Nonequilibrium," *International Journal of Numerical Methods in Heat and Fluid Flow*, Vol. 14, No. 4, 2004, pp. 538–558.

[38]Saad, Y., *Preconditioned Krylov Subspace Methods: An Overview*; Computational Fluid Dynamics Review 1995, Wiley, New York, 1995.